Modeling and Simulation of Water Evaporation from a Droplet of Polyvinylpyrrolidone (PVP) Aqueous Solution

S. R. Gopireddy* and E. Gutheil
Interdisciplinary Center for Scientific Computing, Heidelberg University, Germany
srikanth.reddyg@iwr.uni-heidelberg.de and gutheil@iwr.uni-heidelberg.de

Abstract

This paper presents a model to describe the evaporation and drying behavior of a single quiescent spherical bi-component droplet containing evaporating liquid and dissolved solid substance. Although, many models are available in literature for droplet evaporation and drying, no appropriate model is available to study the liquid evaporation of a polymer aqueous solution. The present study concerns the evaporation and drying of a droplet of polymer (Polyvinylpyrrolidone - PVP) in the solvent water. The water evaporation rate from the droplet is computed using a modification of Abramzon and Sirignano's convective two-film model, and variable liquid and film properties are considered. The effect of PVP presence on vapor pressure of water is estimated by calculating the activity coefficient of water using the UNIFAC-vdW-FV method. The system under consideration is governed by the continuity (diffusion) and energy equations, which are solved using a finite difference method. The simulation results reveal that, as the water evaporates, the droplet starts to shrink and a concentration gradient develops inside the droplet. During the shrinkage, the droplet is assumed to maintain spherical shape. When the solute (PVP) concentration further increases at the surface, the molecular entanglement of polymer commences and thereby starts a solid layer formation on the surface. This solid surface hampers the further solvent evaporation causing the droplet temperature to raise. The effect of drying conditions such as gas velocity and temperature, and relative humidity on evaporation and drying rate is also studied. It is concluded that the present model effectively captures the initial stages of single droplet drying.

Introduction

Spray drying is a primary process for manufacturing the powders where an atomized liquid feed is exposed to hot gas to yield dried material. This is a unique technique, which couples the concurrent processes of solvent evaporation and particle formation involving mass and heat transfer. Although modeling of spray drying has been subject of research for many years, none of the models are applied to a polymer-dissolved-in-water droplet because of the unknown behavior, unavailability of experimental results and complexity of the problem.

Single droplet evaporation and a drying concept are first presented by Charlesworth and Marshall [1] by experimentally measuring the change in droplet mass using the deflection of a thin, long glass filament. This study [1] also classifies different stages of droplet evaporation. Later, this experiment with some modifications is considered in many studies. The work of Sano and Keey [2] includes the drying behavior of colloidal material into a hollow sphere by considering the migration of solid matter towards the center of the droplet through the convection measurement inside the droplet, which is a challenge to experiment [3]. Most of the experiments concerning the droplet evaporation and drying available in literature are either related to salts [1, 4, 5], milk powders [6, 7] or some other colloidal matter [2, 3, 8, 9] and none deal with polymer solutions. Previously developed models assume uniform temperature gradient within the droplet and neglect the effect of solid formation on surface [3, 4, 8]. The study of Nesic and Vodnik [3] presents kinetics of droplet evaporation to predict the drying characteristics of a colloidal silica droplet, where the crust formation on the surface, which occurs in this configuration, is considered. The surface vapor concentration of evaporating solvent is calculated using experimentally measured material dependent factors, which are not available for polymer solutions, where molecular entanglement leads to solid layer formation. Nesic and Vodnik [3] use a more detailed description of various stages of droplet evaporation and drying. Farid [7] shows that the droplet evaporation and drying are controlled by thermal-diffusion rather than mass-diffusion as assumed by most of the earlier studies [1, 2, 4]. In Farid's model [7], the droplet center is always assumed to be at wet-bulb temperature until complete solvent evaporation. The time of crust formation of a colloidal silica droplet is calculated using the energy balance which does not account for solvent and solute composition changes, and the evaporation rate is computed using simple relation without accounting the variation in film and liquid properties. For droplets with initial solids inside, the population balance approach is recently developed [9] to model the nucleation and growth of suspended solids inside an ideal binary liquid droplet with

*Corresponding author: srikanth.reddyg@iwr.uni-heidelberg.de

an assumption that there exists some nuclei of suspended solids initially, but this method cannot be applied in the present case of droplet with polymers dissolved in water.

The aim of the present study is to develop a mathematical model, which can be applied to predict the evaporation and drying characteristics of polymer in water droplets. Prerequisites of the method are inclusion of the solid layer formation at the polymer droplet surface and treatment of the liquid mixture as real through use of the activity coefficient of the evaporating component.

Mathematical Formulation

The problem under consideration is the evaporation and drying of an isolated single spherical droplet consisting of a binary mixture of a liquid and a dissolved solid material with low or zero vapor pressure. The present section presents the general mathematical formulation for an evaporating and drying droplet, but the primary focus is the drying behavior of a PVP in water droplet.

The evaporation rate is calculated based on Abramzon and Sirignano's model [10] with modifications in order to account for the resistance due to solid formation at the droplet surface in evaporation rate as well as temperature equations. During the evaporation and drying, the droplet undergoes four stages as explained by Nesic and Vodnik [3]. In the initial stage, the droplet temperature quickly changes to an equilibrium temperature, which is most often near to the wet bulb temperature for surrounding gas and humidity, with some solvent evaporation. In the second stage, the droplet starts to shrink as solvent evaporates and solute mass fraction raises at the surface, this leads to slight raise in the droplet temperature. The increase in solute mass fraction at the droplet surface hinders the further evaporation rate as vapor pressure of the solvent at the surface drops. The third stage of drying starts when the solute mass fraction at the surface raises to a threshold value, which is most often equal to saturation solubility of the solute in the solvent, where upon the crust formation starts for salts and colloidal material and in the case of polymers, molecular entanglement and gradual increase in concentration lead to solid layer formation at the surface. In the latter case, the solid layer thickens and develops into the droplet interior, and a rapid fall in evaporation rate is observed. In this period, the heat penetrated into the liquid is used for heating the droplet implying the droplet temperature to raise rapidly. Further drying behavior of droplet depends on the vapor diffusivity through the solid layer. In the final stage of drying, boiling followed by particle drying, eventually leading to dried product formation, takes place. In this work, the drying dynamics from the initial temperature change to molecular entanglement causing solid layer formation is simulated.

The problem of evaporation and drying of single droplet can be well defined using the heat conduction and the diffusion equations in spherical coordinates. The heat conduction equation, describing the conductive heat transfer within the droplet, is written as

$$\frac{\partial T}{\partial t} = \frac{\alpha}{r^2}\Big[\frac{\partial}{\partial r}\Big(r^2\frac{\partial T}{\partial r}\Big)\Big], \tag{1}$$

where T is the liquid temperature, α denotes the thermal diffusivity, r is the radial coordinate, and t stands for time. The above equation is solved with the following initial and boundary conditions. At t = 0, the droplet is at uniform temperature, $T = T_0$. At the droplet center, r = 0, zero gradient condition prevails at any time, $\partial T/\partial r = 0$.

The energy balance at the droplet surface is given through the boundary condition

$$-k\frac{\partial T}{\partial r} = h(T_s - T_\infty) \tag{2}$$

at $r = R$, where R denotes the droplet radius. In Eq. (2), T_s denotes droplet surface temperature, and T_∞ stands for gas temperature in the bulk.

First, Equation (1) with initial and boundary condition given in Eq. (2) is solved using a finite difference method to find the temperature gradients inside the droplet. It is observed that the droplet interior temperature responds very quickly to the bulk gas temperature, and the temperature variation from the droplet surface to its center is very small. Therefore, in the remaining simulations, uniform temperature within the droplet is assumed, and the corresponding energy equation is given below, see Eqs. (12) and (13).

The diffusion equation for the substance i in the droplet is formulated in terms of mass fraction Y_i, reads as,

$$\frac{\partial Y_i}{\partial t} = \frac{D_{12}}{r^2}\Big[\frac{\partial}{\partial r}\Big(r^2\frac{\partial Y_i}{\partial r}\Big)\Big], \quad i = 1, 2, \tag{3}$$

where D_{12} is the binary diffusion coefficient in the liquid. In this equation i = 1 denotes the solvent (water) and i = 2 denotes solute (PVP). Equation (3) is numerically solved at every time and spatial location using a finite difference method along with the proper initial and boundary conditions. Initially, the droplet is a homogenous

mixture, $Y_i = Y_{i0}$ at t = 0. At the droplet center, r = 0, the regularity condition must be satisfied at any time, $\partial Y_i/\partial r = 0$. The boundary condition at the droplet surface must account for the change in droplet size, and it is written as,

$$-D_{12}\frac{\partial Y_i}{\partial r} - \frac{dR}{dt}Y_i = \frac{\dot{m}_i}{A\rho_l} \tag{4}$$

at $r = R(t)$. Here $\dot{m}_i$ is the mass evaporation rate of substance i across the droplet surface, $R(t)$ and A are time dependent droplet radius and surface area, respectively, and ρ_l is the liquid density. $\dot{m}_i$ is zero for non-evaporating solute (PVP), $i = 2$. The diffusion Eq. (3) gives the concentration profiles inside the droplet. For solving this equation, the evaporation rate from the droplet surface, $\dot{m}_i$, is needed which appears in Eq. (4). This rate of evaporation is determined based on Sherwood analogy of Abramzon and Sirignano's model [10], and in the present study, it is used in the extended form for bi-component liquid mixture developed by Brenn *et al.* [11], as

$$\dot{m} = \sum_{i=1}^{N=2} \dot{m}_i = [2\pi R_i \bar{\rho}_f \bar{D}_f \widetilde{\mathrm{Sh}} \ln(1 + B_{M,i})], \tag{5}$$

where R_i is volume equivalent partial radius of component i, based on its corresponding volume fraction, computed as $R_i = R(V_i/V)^{1/3}$, $\bar{\rho}_f$ and $\bar{D}_f$ are the density and mass diffusivity in the film, respectively, and $\widetilde{\mathrm{Sh}}$ is modified Sherwood number, $B_{M,i}$ is the Spalding mass transfer number for component i, which is calculated as [10, 12]

$$B_{M,i} = \frac{Y_{i,s} - Y_{i,\infty}}{1 - Y_{i,s}}. \tag{6}$$

Modified Sherwood and Nusselt numbers, which will appear later in the heat transfer rate equation, are expressed as defined by Abramzon and Sirignano [10],

$$\widetilde{\mathrm{Sh}} = 2 + (\mathrm{Sh}_0 - 2)/F_M \quad \text{and} \quad \widetilde{\mathrm{Nu}} = 2 + (\mathrm{Nu}_0 - 2)/F_T. \tag{7}$$

Nesic and Vodnik [3] implemented a similar approach, but they do not account for the volume fraction based radius in the calculation of the evaporation rate, i.e., droplet radius R is used instead of R_i in computing $\dot{m}$. Since the solute vapor pressure is low or zero and the droplet's solute evaporation rate becomes very small, negligence of the volume correction (using R in the place of R_i) may lead to an increased evaporation rate. In the present situation, the summation in Eq. (5) is only over component 1, because PVP does not evaporate, but for the sake of generality, the summation is kept in writing in Eq. (5). The evaporation rate reduction due to solid layer resistance is considered in Eq. (4), and it can be expressed similar to the work of Nesic and Vodnik [3] by,

$$\dot{m}_i = \frac{\sum_{i=1}^{N} [2\pi R_i \bar{\rho}_f \bar{D}_f \widetilde{\mathrm{Sh}} \ln(1 + B_{M,i})]}{1 + \frac{\widetilde{\mathrm{Sh}}\bar{D}_f}{2D_s}\frac{\delta}{R-\delta}}, \tag{8}$$

where δ is the solid layer thickness at the droplet surface and D_s is the diffusivity of vapor in solid layer, which is most often larger than the convection-diffusion coefficient, i.e., $\widetilde{\mathrm{Sh}}\bar{D}_f$ [3]. During the initial stage, δ is zero but once the solid layer has developed on the droplet surface, it offers significant resistance to evaporation which is evident from the second term in the denominator of Eq. (8). The droplet temperature continuously changes due to heat transfer from ambient gas to the binary liquid droplet, and it is computed using the energy balance across the droplet, which gives the net heat transferred into the droplet [10], as

$$Q_L = \dot{m}\Big[\frac{\bar{C}_{p_L}(T_\infty - T_s)}{B_T} - L(T_s)\Big], \tag{9}$$

where B_T is the Spalding heat transfer number, $L(T_s)$ is the latent heat of vaporization of liquid at the droplet surface temperature T_s. Here, the heat transfer number, B_T, is calculated using the following relation [10]

$$B_T = (1 + B_M)^{\phi} - 1, \tag{10}$$

where the exponent ϕ is given as [10],

$$\phi = \frac{\bar{C}_{p_L}}{\bar{C}_{p_g}}\frac{\widetilde{\mathrm{Sh}}}{\widetilde{\mathrm{Nu}}}\frac{1}{\mathrm{Le}}. \tag{11}$$

The time evolution of droplet temperature is calculated by

$$\frac{dT_s}{dt} = \frac{Q_L}{mC_{p_L}}. \tag{12}$$

Equation (12) can be modified to account for the solid layer formation at the droplet surface, and it is written in terms of the solid layer thickness, δ, as

$$\frac{dT_s}{dt} = \frac{1}{mC_{p_L}}\Big[\frac{Q_L + \dot{m}L(T_s)}{1 + \frac{\widetilde{\mathrm{Nu}}\bar{k}_g}{2k_s}\frac{\delta}{R-\delta}} - \dot{m}L(T_s)\Big]. \tag{13}$$

Similar to Eq. (8), the second term in denominator inside the bracket of Eq. (13) denotes the resistance due to solid formation at the droplet surface, and its effect becomes significant only when δ is non–zero. The difference between heat transfer and mass transfer resistance is that the ratio of diffusion coefficients D_{12}/D_s is larger than the ratio $\bar{k}_g/k_s$ [3]. The solid layer thickness δ is computed based on the solute mass balance inside the droplet similar to the work of Nesic and Vodnik [3], and it is given as

$$m_2 = \frac{4}{3}\pi\rho_l Y_2(R-\delta)^3 + m - \frac{4}{3}\pi\rho_l(R-\delta)^3, \tag{14}$$

where m is the total droplet mass, m_2 is the total solute mass in the droplet and Y_2 is the mass fraction of solute (PVP) in the liquid droplet of size $R-\delta$. The first term in right hand side of Eq. (14) is the mass of PVP in the solution and combination of last two terms represents the PVP mass in solid layer. This equation can be solved to get δ.

The presence of polymer with water inside the droplet leads to non-ideal liquid behavior, which must be accounted for in calculating the vapor pressure of water at the droplet surface. In this work, the liquid mixture is treated as real by determining the influence of individual components on each other through their activity coefficients. The activity coefficient of water is computed using the UNIFAC-van der Waals-Free Volume method also known as UNIFAC-vdW-FV method [13].

Before implementation of this advanced method into the current droplet code, it has been verified by comparing it with the well known UNIFAC method [14]; results from these two methods are compared with experimental results from Striolo and Prausnitz [15]. Molecular properties data such as van der Waals volume and radii for PVP polymer are taken from [16, 17], and the other properties required in the UNIFAC-vdW-FV method are taken from [18]. In Fig. 1, the weight based water activity is shown at temperatures of 73°C (left) and 94.5°C (right). For this purpose, water activity, a_w, computed from UNIFAC-vdW-FV method is converted to the activity coefficient, $\gamma_i, i = 1$, using water weight fraction, w_1, and its mole fraction, $x_{L,1}$, where L refers to the liquid, through the relation given as

$$\gamma_i = \frac{a_w w_i}{x_{L,i}},\ i = 1. \tag{15}$$

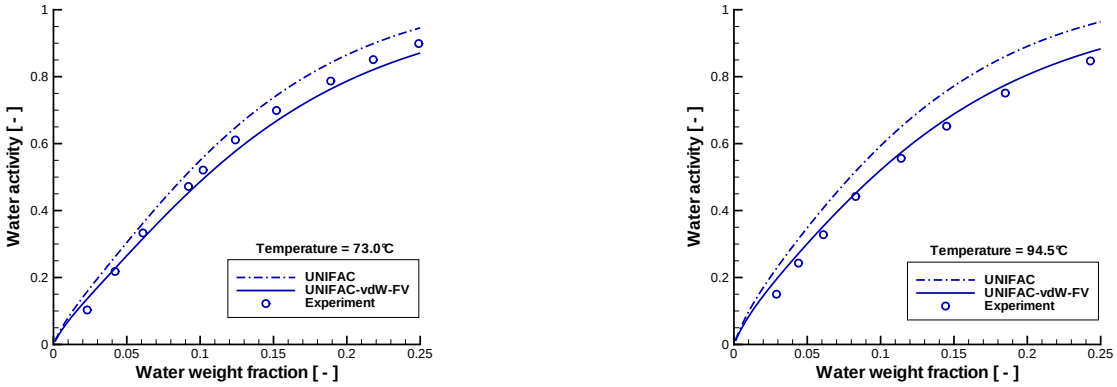

Figure 1. Numerical and experimental [15] results of water activity in PVP/water solution at 73°C (left) and 94.5°C (right)

It is observed that the UNIFAC-vdW-FV method improves the UNIFAC method results, and the UNIFAC-vdW-FV method results in profiles which are in excellent agreement with the experimental data [15]. Therefore, the UNIFAC-vdW-FV method will be used in the remainder of the study.

In the present formulation, the activity coefficient, $\gamma_i, i = 1$, is needed for the calculation of Spalding's mass transfer number, $B_{M,1}$, c.f. Eq. (6), in which the mass fraction, $Y_{1,s}$, of the evaporating component appears; this mass fraction is calculated through the mole fraction, $x_i, i = 1$, of the evaporating component water, in terms of the activity coefficient γ_1, which is written as,

$$x_i = \frac{p_{\mathrm{vap},i}}{P_m}\gamma_i x_{L,i},\ i = 1, \tag{16}$$

where $p_{\mathrm{vap},1}$ is the vapor pressure of pure water and P_m is the total mixture pressure, which is equal to the ambient gas pressure; in the present study it equals the atmospheric pressure.

Results and Discussion

The numerical simulations are carried out by solving Eqs. (3), (8), and (13) simultaneously using a finite difference method. Grid independency of the computational scheme has been assured. Simulations are carried out with different surrounding gas temperatures, gas velocity, and relative humidity to investigate their effect on drying characteristics. The droplet is assumed to be spherical during the entire evaporation and drying processes. The thermal properties of PVP are taken from [19], viscosity and diffusivity of PVP in water are taken from [20], and the remaining other properties are taken from [18]. The diffusion coefficient D_s is not available in literature, therefore, based on [3], it is assumed to be $2\ \widetilde{\mathrm{Sh}} D_f$, and similarly the unknown thermal conductivity, k_s, is taken as $10\ k_g$. The physical and thermal properties in the film are calculated at the reference composition using the $1/3$ rule [21]. The maximum solubility of PVP is not available in literature, and it is assumed to be 30 g in 100 ml water following Bühler [22], which corresponds to a PVP mass fraction of about 0.235.

In Fig. 2, the mass and temperature profiles inside the droplet are shown. Here the droplet initial radius is 200 μm, initial temperature of 20°C, and the surrounding nitrogen gas is flowing with a velocity of 1 m/s at a temperature of 75°C. It is assumed that there is zero relative humidity, and the droplet is homogenous with initial PVP mass fraction of 0.1, see Fig. 3. Figure 2 reveals that during the initial stage, there is no significant raise in droplet temperature, and total droplet mass reduces due to continuous evaporation. After about 6.5 s, the droplet temperature suddenly raises indicating that the solid layer formation on the droplet surface has started, and evaporation slows down due to the resistance built by the solid layer. Figure 3 shows the profiles of PVP mass fraction inside the droplet at different times. Initially, the PVP mass fraction is assumed uniform inside the droplet, and then the droplet size reduces and there is a development of PVP concentration profile inside the droplet, which can be seen at later times. This profile builds up with time and reaches a saturation level of PVP in water at the droplet surface after about 6.5 s, which is visible in Fig. 2, where the PVP mass fraction at the droplet surface at 7 s has reached the assumed saturation value of 0.235.

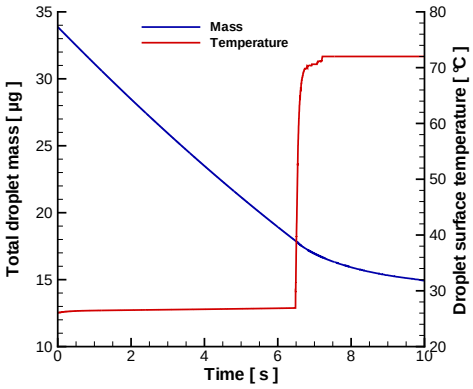

Figure 2. Droplet mass and temperature versus time for a PVP in water droplet at 75°C gas temperature

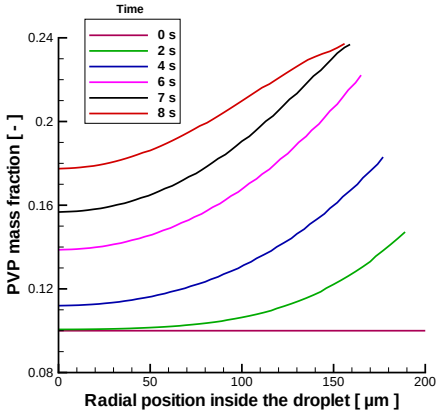

Figure 3. PVP mass fraction profiles inside the PVP in water droplet at 75°C gas temperature

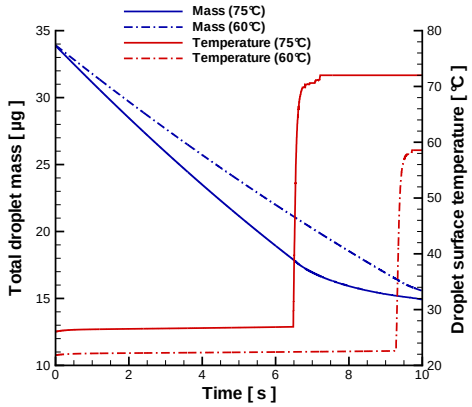

Figure 4. Effect of gas temperature on droplet mass and temperature

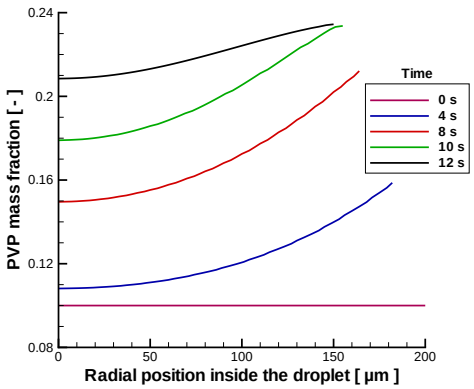

Figure 5. PVP mass fraction profiles inside the droplet at 60°C gas temperature

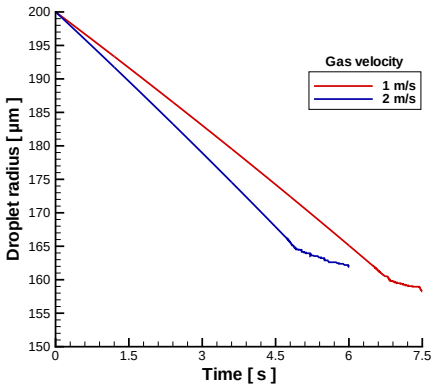

Figure 6. Influence of gas velocity on droplet radius at 75°C gas temperature

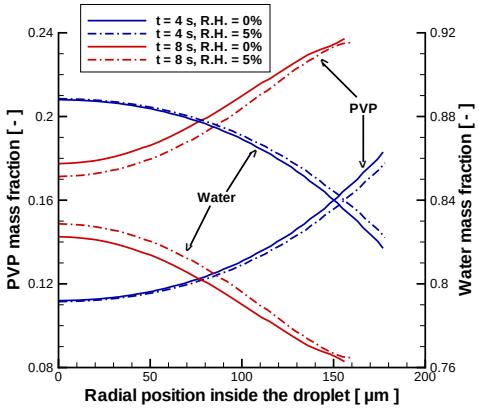

Figure 7. Effect of relative humidity (R.H.) on PVP mass fraction inside the droplet at 75°C gas temperature

Figure 4 gives a comparison of total droplet mass and droplet surface temperature for two different gas temperatures of 60 and 75°C. It can clearly be seen that, the higher the gas temperature the quicker the time taken to see molecular entanglements and to form a solid layer to reduce further evaporation. In case of 60°C, it takes more than 9 s for the droplet temperature to increase, whereas the corresponding value for 75°C is about 6.5 s. Similarly, the reduction rate in total droplet mass slows down. Figure 5 shows the development of PVP mass fraction inside the droplet for 60°C, which can be compared with the situation for 75°C shown in Fig. 3. The mass fraction of PVP at the droplet center reaches 0.15 in 8 s for 60°C gas temperature, whereas for 75°C, it reaches about 0.18 in the same time, because the higher gas temperature yields larger driving force for heat transfer, c.f. Eqs. (9) and (12), into the liquid causing faster evaporation. In Fig. 6, the effect of gas velocity on drying rates is displayed for two different gas velocities of 1 and 2 m/s. It can observed that the droplet size reduces more quickly in the case of higher gas velocity: the larger droplet Reynolds number, c.f. Eq. (8), causes a higher loss of evaporating component in the droplet as gas velocity increases. After some time, the decrease in droplet size retards because of the solid layer formation as observed in Fig. 4. Solid layer formation occurs at around 7 s for 1 m/s conforming with Fig. 4, and in 4.5 s for 2 m/s (not shown). Hence, the effect of gas velocity on droplet drying characteristics is very significant.

The influence of relative humidity of 5% in the surrounding gas on droplet evaporation and drying is shown in Fig. 7 for 75°C gas temperature flowing at 1 m/s. The times of 4 s (blue lines) and 8 s (red lines) are displayed. The no humidity condition (solid lines) is also shown for purpose of comparison. The PVP mass fraction is lower for higher relative humidity, whereas the water mass fraction is higher due to the smaller driving force for the mass transfer, see Eq. (6), delaying water evaporation. The differences between no humidity and 5% humidity situations

build up with time: at 4 s, the droplet interior is hardly affected, and humidity starts influencing the outer region inside the droplet. At a later time, $t = 8$ s, the differences are large in the droplet core, and they are reduced towards the droplet surface, where the saturation solubility is reached.

The study shows the UNIFAC-vdW-FV method to greatly improve the results of the UNIFAC method. Droplet humidity, and both gas velocity and temperature strongly affect PVP/water droplet drying characteristics. A more detailed knowledge of saturation solubility and the diffusivity of vapor through the solid layers as well as its thermal conductivity is desirable, and experiments are strongly encouraged to gain these data.

Summary and Conclusions

In this study, a model to describe the evaporation and drying of the polymer PVP in water is developed. The system under consideration is governed by the continuity (diffusion) and energy equations. The evaporation rate of water from the droplet at a given time is calculated using a modification of Abramzon and Sirignano's model [10], which includes the volume fraction based droplet radius [11] and resistance from solid layer. The temperature inside the droplet is assumed to be uniform, and the change in droplet temperature due to heat penetration through the droplet surface from the surrounding gas is calculated with similar modifications used for mass evaporation rate, and resistance from the solid layer is formulated following Nesic and Vodnik [3]. The liquid mixture is treated as real with the activity coefficient calculation using the improved UNIFAC-vdW-FV method.

The results show that both the gas temperature and velocity have significant influence on the evaporation and drying characteristics of PVP in water droplet. PVP in water evaporation and drying have similar behavior for droplet mass and temperature evolution with time compared to other material such as silica gel [3]. However, the crust building in silica gel is not present here, and molecular entanglement and solid layer formation occur for the PVP in water droplet studied here. The relative humidity plays a major role in the mass fraction gradients and the results are analogues to the previous results of Brenn *et al.* [11] for the droplet evaporation of two liquid components.

The present model lacks experimental information of saturation solubility and the diffusivity of vapor through the solid layers as well as its thermal conductivity, these values were estimated in the present study. Experiments are strongly encouraged to gain these data.

Acknowledgements

The authors gratefully acknowledge the financial support from Deutsche Forschungsgemeinschaft (DFG) through SPP 1423 and Graduate School MathComp at IWR of Heidelberg University. They thank N. Wenzel for the assistance in data processing and R. P. Danner from Pennsylvania State University, for providing details of UNIFAC-vdW-FV method. The careful review of the present paper by ICLASS 2012 reviewers is also gratefully acknowledged.

References

[1] Charlesworth, D. H., Marshall, W. R. Jr, *AIChE Journal* 6: 9-23 (1960).
[2] Sano, Y., Keey, R. B., *Chemical Engineering Science* 37: 881-889 (1982).
[3] Nesic, S., Vodnik, J., *Chemical Engineering Science* 46: 527-537 (1991).
[4] Brenn, G., *Chemical Engineering and Technology* 27: 1252-1258 (2004).
[5] Seydel, P., Blomer, J., Bertling, J., *Drying Technology* 24: 137-146 (2006).
[6] Chen, X. D., *Drying Technology* 22: 179-190 (2004).
[7] Farid, M., *Chemical Engineering Science* 58: 2985-2993 (2003).
[8] Nesic, S., *Drying* 89: 386-393 (1989).
[9] Handscomb, C. S., Kraft, M., Bayly, A. E., *Chemical Engineering Science* 64: 628-637 (2009).
[10] Abramzon, B., Sirignano, W. A., *International Journal of Heat and Mass Transfer* 32: 1605-1618 (1989).
[11] Brenn, G., Deviprasath, L. J., Durst, F., *Proc. 9th International Conference on Liquid Atomization and Spray Systems, Sorrento, Italy*, 2003.
[12] Kastner, O., *Theoretische und experimentelle Untersuchungen zum Stoffübergang von Einzeltropfen in einem akustischen Rohrlevitator*, PhD thesis, University of Erlangen-Nürnberg, Germany, 2001.
[13] Kannan, D. C., Duda, J. L., Danner, R. P., *Fluid Phase Equilibria* 228-229: 321-328 (2005).
[14] Fredenslund, Aa., Jones, R. L., Prausnitz, J. M., *AIChE Journal* 21: 1086-1099 (1975).
[15] Striolo, A., Prausnitz, J. M., *Polymer* 41: 1109-1117 (2000).
[16] Bondi, A., *Physical properties of molecular crystal, liquids and glasses*, Wiley, New York, 1968.
[17] Danner, R. P., High, M. S., *Handbook of polymer solution thermodynamics*, DIPPR Project, AIChE, New York, 1993.

[18] Daubert, T. E., Danner, R. P., *Data compilation of properties of pure compounds*, DIPPR Project, AIChE, New York, 1985-1992.
[19] Dakroury, A. Z., Osman, M. B. S., El-Sharkawy, A. W. A., *International Journal of Thermophysics* 11: 515-523 (1990).
[20] Metaxiotou, Z. A., Nychas, S. G., *AIChE Journal* 41: 812-818 (1995).
[21] Yuen, M. C., Chen, L. W., *Combustion Science and Technology* 14: 147-154 (1976).
[22] Bühler, V., *Polyvinylpyrrolidone excipients for pharmaceuticals*, Springer, 2005.